Journal of Applied Polymer Science

The Polymer Free Volume as a Controlling Factor for Drug Release from Poly(lactide-co-glycolide) Microspheres

Stefan Scheler
Sandoz GmbH, Sandoz Development Center Austria, Austria, Kundl 6250, Austria
Correspondence to: S. Scheler (E-mail: stefan.scheler@t-online.de)

ABSTRACT: Drug release from poly(lactide-*co*-glycolide) (PLGA) microspheres is strongly determined by the pore structure of the particles. This study examines how swelling-induced pore constriction delays the drug release and by which factors this process is controlled. Combination of different porosimetric and pycnometric methods enabled insight into the submicroscopic range of the pore structure and revealed that remarkably the polymer free volume plays a crucial role in drug release from PLGA microspheres. Surprisingly, the latter was shown to be inversely correlated to the degree of diffusional drug release. This can be explained by a swelling-induced constriction of the macroporous channel system in the microspheres which is related to the availability of free volume. The hole free volume was shown to be well controllable by the manufacturing conditions. Thus, the study deepens comprehension of the mechanism of drug release from biodegradable microparticles and offers an effective approach for controlling the release behavior. © 2013 Wiley Periodicals, Inc. J. Appl. Polym. Sci. 000: 000–000, 2013

KEYWORDS: drug delivery systems; polyesters; porous materials

Received 14 February 2013; accepted 6 July 2013; Published online
DOI: 10.1002/app.39740

INTRODUCTION

The great potential of biodegradable polymer microspheres for pharmaceutical applications has been recognized since the 1960s. Since then, a huge number of therapeutic options and the encapsulation of a large variety of different drugs have been studied. Microspheres were found to be applicable as carriers for small molecules, peptides, proteins, vaccines, and even nucleic acids.[1–4] Administration routes tested comprise oral, parenteral, nasal, pulmonary, intraocular, and vitreoretinal drug delivery.[5–10] Strong efforts were made to understand the complex mechanisms governing drug release from microparticles and to optimize release kinetics. However, despite almost half a century of research, the process of drug release from microparticles is still not fully understood in detail. Perhaps more than in case of many other dosage forms the release pattern from microparticles is strongly determined by the microscopic and submicroscopic structure of the particle matrix. As these structural features are generated during the particle formation, process parameters have an enormous influence on drug release *in vitro* and *in vivo*.

Emulsification of a polymer solution in an aqueous continuous phase followed by the removal of the organic solvent is one of the most common techniques for the preparation of biodegradable microparticles. Drug release from those microspheres is a highly complex multistage process. Numerous interactions between many different factors, most of them changing over the release period, make comprehension difficult. The release process is controlled by diffusion and erosion processes. In case of poly(lactide-*co*-glycolide) (PLGA) particles, the mechanism was shown to be of the bulk erosion type as the polymer degradation process is the speed determining step.[11] The particles are homogenously invaded by water prior to significant degradation. Cleavage of ester bonds creates free carboxylic acid groups at the newly formed chain ends which partly dissociate and thus decrease the pH of the water imbibed by the particles. The ester hydrolysis is an acid-catalyzed process and will accelerate in an acidic environment. If a particle is surrounded by a neutral medium and free diffusion is inhibited within the particle matrix, a pH gradient will develop from the particle surface to the core, leading to an increased degradation rate in the center. However, microparticles prepared by solvent extraction/evaporation usually have a highly porous matrix structure which should neither be able to significantly restrict the leaching of drugs and polymer degradation products from the particles into the surrounding medium nor the diffusion of buffer salts from the medium into the particles.[12] For this reason, it is remarkable that, despite of a porous structure and even a porous surface, in many cases the drug release profiles reveal a slow or even delayed onset.[13–17] Such a pattern would be expected in case of a tightly packed polymer matrix but not in case of a highly porous, sponge-like structure.[18,19]

For a long time, drug diffusion through the polymer matrix or through pre-existing pores followed by an erosional expansion and opening of the pore structure was regarded as the reason for the typical and often multistage release profile.[20] In these models, it was assumed that only small pores become enlarged and isolated pores become open, but not *vice versa*. However, during the last years, the perception gained ground that not only opening of pores but also pore closure takes place during drug release from microspheres.[19,21–25] Such type of mechanism would be able to explain the release behavior discussed above. This study was made to prove this assumption and, most importantly, to identify the factors governing the closure of pores.

The first part of the study is dedicated to the question whether indications can be found confirming the involvement of a pore closure mechanism in drug release. Such indications were tried to be deduced from the kinetics of drug release and water uptake. In particular, the question was raised whether the drug release takes place through the polymer matrix or via water-filled pores. If it could be shown that, despite the existence of a clearly visible network of large interconnected pores in the dry state, the drug diffuses to the surface on a pathway through the polymer, this would provide a strong indication that the porous network becomes closed upon water uptake.

This would raise the question, which factors and mechanisms are controlling this process. Based on a series of equally composed microparticles differing only in terms of their porosity profiles, in the second part of the study it was investigated, if structural features can be identified correlating with the rate and degree of diffusional drug release. Under the aforementioned assumption, that the obstruction of the pore channels forces the drug to take the much slower diffusion path through the polymer, the extent of diffusional release prior to the commencement of the erosional phase can be considered as a measure of the effectiveness of pore closure. The most obvious reason for such an obstruction of intraparticulate voids is the swelling of the polymer. Thus, it was particularly searched for structural elements linked to the rate and extent of water distribution within the polymer and to the ability to expand the network of molecular chains.

EXPERIMENTAL

Materials

The model drug 3-{2-[4-(6-fluor-1,2-benzisoxazol-3-yl)piperidino]ethyl}-2-methyl-6,7,8,9-4-H-pyrido[1,2-a]pyrimidin-4-one was obtained from Jubilant Organosys (Mysore, India). Poly(D,L-lactide-*co*-glycolide) 75:25 (Resomer 755 S), $M_w = 58{,}300$ Da was purchased from Boehringer Ingelheim (Ingelheim, Germany). Polyvinylalcohol 18–88 was a grant from Kuraray Europe GmbH (Frankfurt am Main, Germany). Methylene chloride analytical grade was obtained from Merck (Darmstadt, Germany) and (*Tris*(hydroxymethyl)-aminomethane) (TRIS) from AppliChem (Darmstadt, Germany).

Microparticle Preparation

An emulsification, solvent extraction/evaporation method was used for microparticle preparation as described by Vay et al.[12] In brief, a solution of 2.8 g drug substance and 3.2 g PLGA in 40 mL methylene chloride was emulsified by static mixing with 500 mL of a 0.5% w/v aqueous solution of polyvinylalcohol buffered with 0.1*M* TRIS (pH 9.0). After feeding the emulsion into 3.5 L of additional aqueous phase, the solvent was removed at different temperatures (10–35°C) from the droplets by stirring (230 or 260 rpm) and, in case of using a closed reactor, by headspace ventilation (10 L/min). The hardened particles were harvested by filtration and vacuum dried.

Drug Load and *In Vitro* Drug Release

The drug load of the microspheres was determined by high-performance liquid chromatography (HPLC) (RP 18 column 20 × 2.1 mm, mobile phase 75:25 v/v mixture of 0.25*M* phosphate buffer (pH 8.5) and acetonitrile, flow rate 1 mL/min) after dissolving the particles in acetonitrile and diluting with 0.1*N* HCl. *In vitro* drug release was tested under sink conditions by agitating microparticle samples in phosphate buffer solution, pH 7.4, at 37°C using an orbital shaker. In predefined intervals, samples of 0.2 mL were drawn from the medium for HPLC measurement of the drug concentration.

Water Uptake

Water uptake of the microparticles was measured from samples incubated for different times at 37°C in phosphate buffer solution, pH 7.4, on a heated orbital shaker. After determination of the dry tare weight of Vivaclear Centrifugal Filters (Sartorius Stedim Biotech GmbH, Goettingen, Germany), they were wetted with the buffer solution, centrifuged for 5 min at 6000 rpm to remove the noncapillary bound water, and weighed again to obtain the tare weight of the wetted filters. Then, samples of the particle suspensions were transferred into the filters and dewatered by centrifugation under the same conditions as described above. After weighing the filters with the wet particles, they were dried for 24 h in a desiccator at room temperature and weighed again. The water uptake was calculated as the difference between the wet and the dried particles.

A selective determination of the nonbound fraction of water was made by differential scanning calorimetry (DSC) measurement (DSC 823e/500 calorimeter, Mettler Toledo, Greifensee, Switzerland) of the wet particles and analysis of the melting peak at about 0°C. Approximately, 10 mg of the wet sample was weighed into 40 µL aluminum pans and hermetically sealed. As a reference, an empty aluminum pan was used. After cooling to −40°C, the pans were heated at a rate of 10°C/min. The amount of frozen water was calculated from the area of the melting peak on the basis of an enthalpy of fusion of 333 kJ/kg.

Particle Size Measurement

The particle size distribution was measured by single-particle optical sensing (SPOS) using an AccuSizer 780 instrument (Particle Sizing Systems, Santa Barbara, CA) equipped with a LE400-05SE sensor type. This method, which is based on light obscuration, is able to count and size particles from 0.5 to 400 µm. The data are obtained in 512 logarithmically spaced channels with fraction widths ranging from 1 to 5.54 µm.

Porosity Measurement

The porosity distribution of the particles was recalculated from data published in a previous study.[12] The method which we

developed there is based on a combination of gas pycnometry, mercury porosimetry, and single-particle optical sensing (SPOS). In brief, the intraparticulate pore space was gauged by applying three intrusion media with different penetration depths. The exclusion limit of helium and nitrogen in gas pycnometry is defined by the kinetic diameter of the atoms or molecules (He: 0.26 nm, N_2: 0.36 nm) and the cutoff for mercury intrusion is determined by the applied pressure, according to the Washburn equation 3.9 μm at 350 kPa). With each medium, a different particle density was obtained because the particle volume was measured as the sum of the polymer's skeletal volume and a variable volume of inaccessible voids. The envelope volume of the microspheres, which is required to calculate the accessible fraction of the total intraparticulate pore volume as the difference between the total particle volume and the inaccessible volume for each intrusion medium, was measured by SPOS. This method allows quantitatively counting and sizing all particles of a weighed sample. The total particle volume was derived as the sum of the volumes of each microsphere, calculated from the measured diameters, and was finally normalized by the weight. The skeletal volume of the polymer matrix was obtained from the particle weight and the true density of the pure polymer. The instruments used for these measurements were Ultrapycnometer 1000 (Quantachrome GmbH, Odelzhausen, Germany), Mercury porosimeter Pascal 140 (Thermo Fisher Scientific, Milano, Italy), and a single-particle optical sizer AccuSizer 780 (Sensor: LE400-05SE; Particle Sizing Systems, Santa Barbara, CA). More details of the method are described by Vay et al.[12]

Differential Scanning Calorimetry

The glass transition temperature (T_g) of the polymer was determined by DSC using a DSC 823e/500 calorimeter (Mettler Toledo, Greifensee, Switzerland). Approximately, 10 mg was weighed into 40 μL aluminum pans and hermetically sealed. As a reference, an empty aluminum pan was used. A first heating cycle from −40 to 80°C with a temperature ramp of 10°C/min was run to eliminate any sample history. Then, the sample was cooled to −10°C and heated again at the same rate. T_g was determined in duplicate as midpoint temperature using the STAR software (Mettler Toledo, Greifensee, Switzerland).[26]

Time Course of Polymer Degradation

Six samples of about 17 mg of microparticles were incubated in 100 mL phosphate buffer solution, pH 7.4, under the same condition as for the determination of drug release (see above). At each sampling time point, the content of one vessel was vacuum filtered through a polypropylene 12 mL filter tube with a 1.0 μm polytetrafluoroethylene membrane (Whatman GmbH, Dassel, Germany) and washed with 100 mL of water. The residue was dried by sucking air through the filter and storing the filter tube over night in a desiccator. After solving the residue in tetrahydrofuran (THF) containing 0.045% butylhydroxytoluene (BHT, as stabilizer and internal standard), the molecular weight was determined by gel permeation chromatography with refractive index detection. Three columns (300 × 8 mm) with a stationary phase of styrene–divinylbenzene copolymers with different pore sizes (0.1, 10, and 100 μm) were connected in series. Mobile phase: THF stabilized with 0.025% of BHT, injection volume: 100 μL, flow rate: 1.0 mL/min.[26]

Analysis of the Temperature Dependence of Drug Release Kinetics

As the diffusion in solids is an activated process, the diffusion coefficient D is well predicted by a correlation similar to the Arrhenius equation,

$$D = D_0 e^{-E_A/RT} \tag{1}$$

where D_0 is the maximum diffusion coefficient, E_A is the activation energy, R is the gas constant, and T is the temperature.[23,27] A linear relation is obtained if ln D is plotted against $1/T$. According to Fick's first law, the amount of substance diffusing per unit area and unit time (diffusional flux, J) is proportional to the diffusion coefficient if the concentration gradient is constant.[19] As the concentration gradient can be considered as constant during the very first hours of incubation, in which only a small portion of the encapsulated drug (<3%) is released from the particles, a linear relationship is also obtained between ln J and $1/T$. During the first phase of drug release, in which the particles' surface area does not change, also the zero-order rate constant of drug release k (change of drug concentration per time) is linearly correlated to the diffusional flux J and thus to $1/T$:

$$k = k_0 e^{-E_A/RT} \tag{2}$$

Curve Fitting of Dissolution Profiles and Calculation of the Diffusion Coefficient

Diffusional release was modeled by Crank's solution to Fick's second law. As the drug release from degradable microparticles is a multistage process in which the initial diffusion phase is followed by a more or less overlapping accelerated release owing to matrix erosion, Crank's equation was extended by addition of a second term, accounting for the erosional release. In contrast to the diffusion phase (and in order not to unnecessarily complicate the calculation), the erosion phase was modeled in a descriptive way by using a Weibull function to describe the sigmoidal curve shape.[28,29]

$$M_t = M_1^{\infty}\left(1 - \frac{6}{\pi^2}\sum_{n=1}^{\infty}\frac{1}{n^2}e^{-Dn^2\pi^2\left(t-t_{\text{lag}1}\right)/r^2}\right) + \left(M_2^{\infty} - M_1^{\infty}\right) \times \left(1 - e^{-\left(\frac{t-t_{\text{lag}1}-t_{\text{lag}2}}{c}\right)^b}\right) \tag{3}$$

M_t = released drug amount at time t; D = diffusion coefficient; t = time; M_1^{∞} = total releasable amount owing to diffusion; M_2^{∞} = total releasable amount due to diffusion and erosion; $t_{\text{lag}1}$ = lag time before diffusional release; $t_{\text{lag}2}$ = lag time between diffusional and erosional release; r = microsphere radius; b = shape constant; c = scale constant; n = 1–12 (an upper limit of summation of more than 12 was described not to further improve the approximation).[21]

Another model applied for curve-fitting accounts for systems in which the drug load is higher than the solubility of the drug in the carrier matrix. It was developed by Koizumi and Panomsuk and describes the cumulative drug release from a single spherical carrier unit as a function of the radius r of this unit, the initial drug concentration c_0, the drug's solubility c_s within the system, the diffusion coefficient D, and the time t. Dividing this

Table I. Manufacturing Parameters of Studied Preparations

	A1	A2	B1	B2	B3	B4	B5	B6
Pump rate for static mixing (g/min)								
Organic phase	6	9	10	10	10	10	10	10
Aqueous phase	120	180	190	190	190	190	190	190
Stirrer type and stirring speed (rpm)	Propeller 230	Propeller 230	Anchor 260	Anchor 260	Anchor 260	Anchor 260	Anchor 260	Anchor 260
Extraction temperature and duration	22→52°C in 5 h, 52°C for 1 h, 52→22°C in 1 h	22→52°C in 5 h, 52°C for 1 h, 52→22°C in 1 h	10°C, 5 h	20°C, 5 h	27.5°C, 5 h	30°C, 5 h	32.5°C, 5 h	35°C, 5 h
Headspace ventilation (L/min)	Open reactor, no ventilation	Open reactor, no ventilation	10	10	10	10	10	10

function by the average drug load of a single particle and additively combining it with the Weibull term for the erosional release phase provides the following equation for the cumulative drug release M_t at time t.

$$M_t = \frac{3M_1^\infty}{c_0 r}\left[\sqrt{2(c_0-c_s)c_s Dt} + \frac{4c_s Dt}{9r}\left(\frac{c_s}{2c_0-c_s}-3\right)\right] + \left(M_2^\infty - M_1^\infty\right) \times\left(1-e^{-\left(\frac{t-t_{lag1}-t_{lag2}}{c}\right)^b}\right) \quad (4)$$

The diffusion coefficients were calculated by fitting these functions to the measured drug release profiles, using the Solver tool of Microsoft Excel.

RESULTS

Two series of drug-loaded PLGA microparticles were investigated in this study. Both of them were prepared by a solvent extraction/evaporation process, with the batches of the first series (A1–A2) differing in the pump rate for static mixing and the batches of the second series (B1–B6) differing in the extraction temperature (Table I). As was shown in the previous studies, the particle size is mainly determined by the flow velocity in the static mixer, whereas the structural morphology and the drug release profile are substantially controlled by the process temperature during the manufacturing step of solvent removal.[26,30] Thus, in the first series two different flow rates and in the second series six different extraction temperatures were applied to obtain particles with graduated properties. With the differently sized microparticles of the first series (A1–A2), it should be examined if there is evidence that pore closure mechanisms are involved in the drug release process. The second series of particles (B1–B6), with varying porosity profiles, should elucidate how such mechanisms could be possibly related to the structure of the polymer matrix. The particle size and the molecular weight of the polymer matrix are listed in Table II. First, kinetic studies were performed to elucidate the diffusion paths of water and drug substance, then the pore structure of the particles was investigated and finally conclusions were drawn from correlations between diffusion behavior and pore size distribution.

Kinetics of Processes Involved in Drug Release

Rate Constant of Initial Drug Release. In the first part of this study, the drug release under sink conditions at pH 7.4 was studied at different incubation temperatures. Two batches of

Table II. Particle Properties of Studied Preparations

	A1	A2	B1	B2	B3	B4	B5	B6
Particle size (μm) (volume weighted median)	192.2	39.2	82.7	84.4	85.5	82.3	86.8	87.1
σ_ξ (Dimensionless) (calculated for logarithmic distribution)	0.32	0.68	0.27	0.29	0.34	0.34	0.39	0.33
M_w (kDa)	n/a	n/a	54.1	53.6	54.2	53.2	51.0	48.4
Volume of pores <0.26 nm (%)	n/a	n/a	1.1	1.3	n/a	1.8	1.0	1.0
Volume of pores 0.26–0.36 nm (%)	n/a	n/a	0.3	1.6	n/a	6.2	5.5	7.9
Volume of pores 0.36 nm–7.5 μm (%)	n/a	n/a	0.0	1.3	n/a	1.4	1.4	0.0
Volume of pores >7.5 μm (%)	n/a	n/a	20.4	16.8	n/a	10.4	16.7	18.3
Volume of the polymer scaffold (%)	n/a	n/a	78.2	79.0	n/a	80.2	75.4	72.7

n/a: not analyzed.

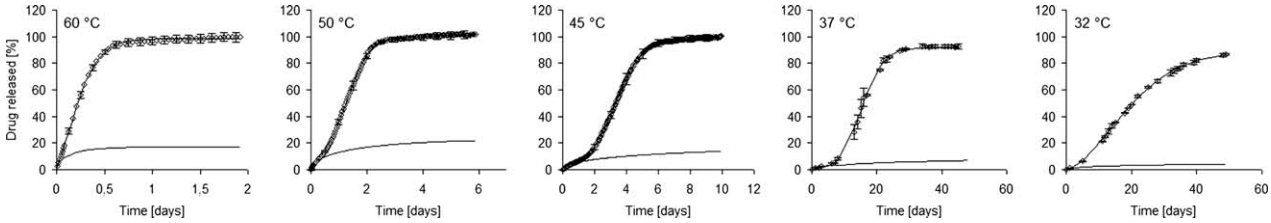

Figure 1. Drug release from preparation A2 (symbols) fitted by eq. (3) (upper curves). The lower curves are calculated from Crank's term of eq. (3) and depict the contribution of diffusional release.

microparticles (A1 and A2) were investigated. The release profiles of preparation A2 measured at 32, 37, 45, 50, and 60°C are shown in Figure 1. The focus was directed on the initial phase of drug release which is governed by a diffusion mechanism. It was found that in the very first phase the cumulative drug release can be approximated by zero-order kinetics ($R^2 > 0.95$) with a rate constant k, calculated as the slope of the concentration/time curve (data not shown). The rate constants obtained at different release temperatures are shown in Figure 2.

Diffusion Coefficient during the Initial Release Phase. If diffusion is the rate-determining process, the diffusion coefficient D can be deduced from the drug release profile by Crank's solution to Fick's second law, which models the diffusional drug release from a spherical matrix.[31,32] As described in the **EXPERIMENTAL** section, the Crank's equation (eq. (3)) was extended by a Weibull term to fit not only the initial diffusion phase but also the more or less overlapping phase of subsequent matrix erosion. These fits are shown in Figure 1 together with the measured release profiles. The graphs of the equation's Crank's term, calculated from the fitted functions, are also exhibited in the diagrams to illustrate the contribution of initial diffusional release. The diffusion coefficients obtained from this fitting process are shown in Figure 3.

Crank's equation was developed for systems in which the drug is molecularly dispersed (solved) within a homogenous matrix. However, as described in a former article, this is only partly true for the microspheres studied in this study.[33] Melting peaks of the drug occurring in DSC thermograms of the particles as well as scanning electron microscopy photomicrographs, revealing crystals embedded in the cavities of a macroporous polymer structure, indicate that at least a portion of the drug is not molecularly dispersed. In a former study, the thermodynamic solubility of the drug within the polymer was calculated from Hansen partial solubility parameters of drug and polymer as 12.6% m/m, which is in close agreement to the value obtained from the heat of fusion of the crystalline drug fraction in the microspheres.[33] This means that, based on a drug load of 39.3% (A1) and 32.3% (A2), only less than one-third of the encapsulated drug (A1: 22.2% of the drug load, A2: 30.2% of the drug load) is solved in the polymer and thus molecularly dispersed.

Different mathematical models have been developed for the calculation of drug release from systems in which the drug load is higher than the solubility of the drug in the polymer matrix. One of these models, developed for carriers of spherical geometry, was reported by Koizumi and Panomsuk.[34] Using this model, about the same diffusion coefficients are obtained (mean deviation 0.3 log steps, max. deviation 0.8 log steps) as with Crank's equation.

The fact that, despite the presence of crystalline drug, Crank's approach provides about the same results as obtained by the method of Koizumi and Panomsuk might be an indication that the first portion of drug, which is released during the

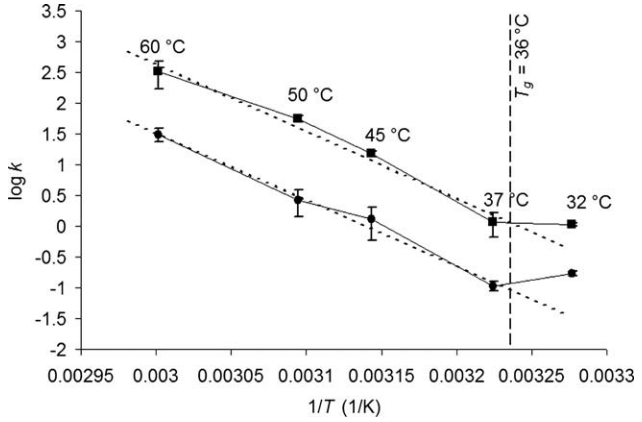

Figure 2. Correlation between the logarithm of the initial drug release rate from the particles (k = rate constant of the initial zero order release) and the reciprocal value of the temperature (sample A1: circles, sample A2: squares). Only the data points above T_g exhibit a linear correlation. The dotted lines are the calculated regression lines for the 37–60°C data.

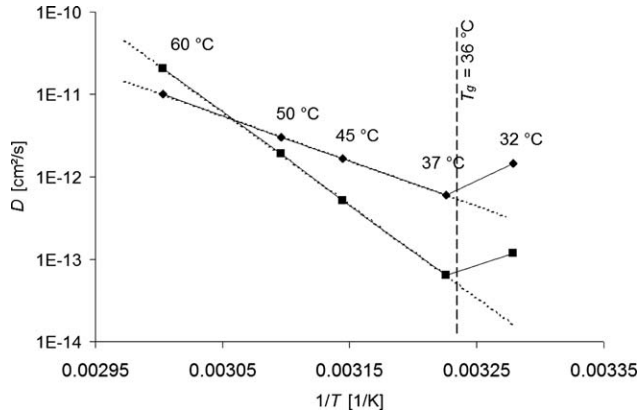

Figure 3. Correlation between the effective diffusion coefficient of the drug within the particle matrix (in logarithmic scale) and the reciprocal value of the temperature (sample A1: circles, sample A2: squares). Only the data points above T_g exhibit a linear correlation. The dotted lines are the calculated regression lines for the 37–60°C data.

Applied Polymer SCIENCE

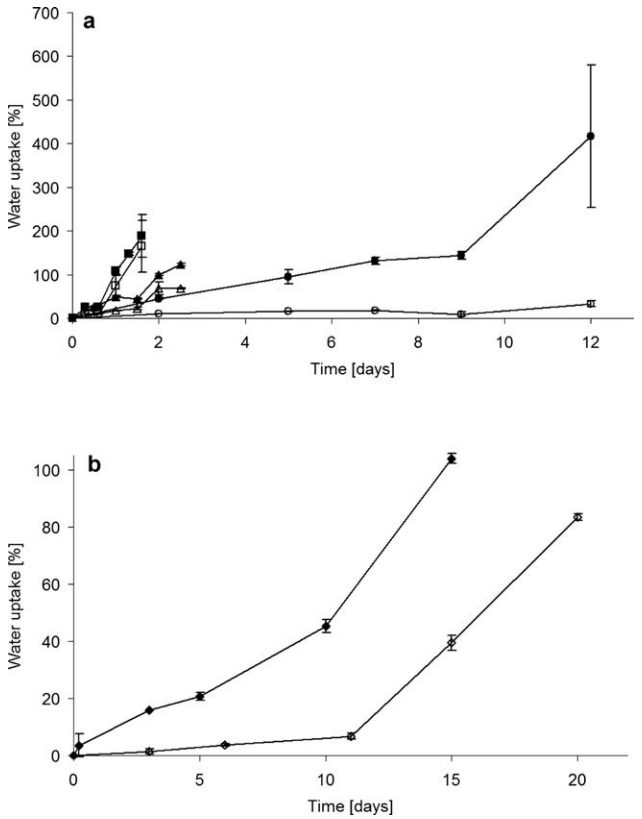

Figure 4. a: Water uptake by particles of preparation A1 (open symbols) and A2 (solid symbols) at different temperatures (32°C: circles, 50°C: triangles, 60°C: squares), b: Water uptake by particles of preparation B1 (open symbols) and B5 (solid symbols) at 37°C.

diffusional phase, probably originates from the dissolved (molecularly dispersed) fraction.

Kinetics of Water Uptake. When the water uptake is studied by measuring the weight gain of the incubated particles it can be observed that, after a fast onset of imbibition, the uptake rate decreases within the first hours or days to about zero before it increases again sharply to a value markedly higher than the initial rate [Figure 4(a)]. As it can be seen from preparations A1 and A2, with rising temperature the initial uptake rate increases, but the uptake ceases earlier and the amount of water imbibed during this initial phase, marked by the height of the temporary plateau, decreases. Similar curve profiles were also measured with other microparticle preparations. Figure 4(b) shows the water uptake of preparations B1 and B5, both tested at 37°C.

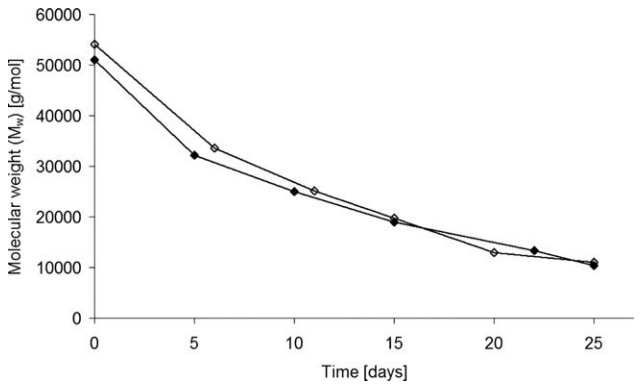

Figure 5. Polymer degradation (molecular weight loss) during incubation of particles in buffer pH 7.4 at 37°C. Preparation B1 (open symbols) and B5 (solid symbols). The relative standard error (RSE) of the method was determined from 30 measurements of a control sample as 0.31%.

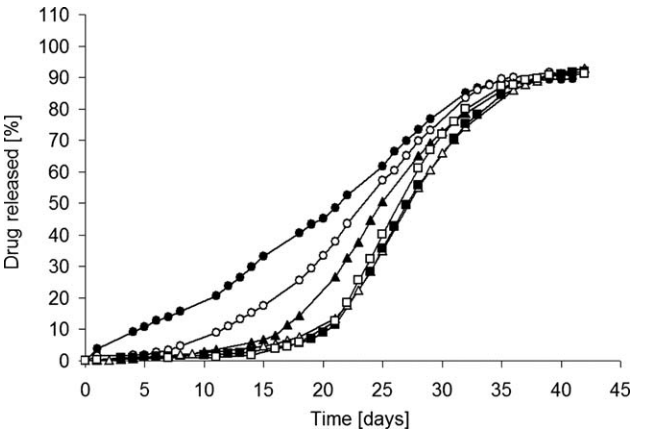

Figure 6. Drug release (pH 7.4, 37°C) from microspheres of preparation B1–B6 at 37°C, pH 7.4: B1 solid circles, B2 open circles, B3 solid triangles, B4 open triangles, B5 solid squares, B6 open squares. The values of B1–B3 are based on single batches which were analyzed in duplicate ($n = 2$). The values of B4–B6 are obtained as averages from two batches, produced with identical process parameters, each of them analyzed in duplicate ($n = 4$). For reasons of clearness, error bars of these curves are only shown in Figure 9.

Kinetics of Polymer Degradation. Polymer degradation of preparations B1 and B5 was studied at pH 7.4 and 37°C (Figure 5). Both curves exhibit nearly congruent profiles. They reveal that degradation starts immediately after incubation. The slightly lower initial value of the B5 curve can be explained by a certain degree of polymer degradation during the particle manufacturing process owing to the higher extraction temperature compared to preparation B1.

Relationship between Drug Release and Particle Structure

Drug Release of Differently Structured Particle Preparations. Figure 6 shows the release profiles (37°C, pH 7.4) of microsphere preparations B1–B6. They are characterized by a three-phase pattern with a more or less pronounced initial lag-time followed by a period of slow release which accelerates after about 20 days. The lower the release rate is in the second phase, the more it accelerates in the third phase. From B1 to B6, the second phase release decelerates, whereas the duration of the lag time and the release rate of the third phase increase. These changes are most pronounced between B1 and B4.

Pore Size Distribution. In many cases, mercury porosimetry, the standard technique for the determination of pore size distribution profiles, is not able to distinguish between inter- and intraparticulate voids, because, especially in heterodisperse particles, the size of the smallest interparticulate voids overlaps with the diameter of the largest intraparticulate pores. For this reason, a method combining low-pressure mercury porosimetry with gas pycnometry and an optically based technique for the

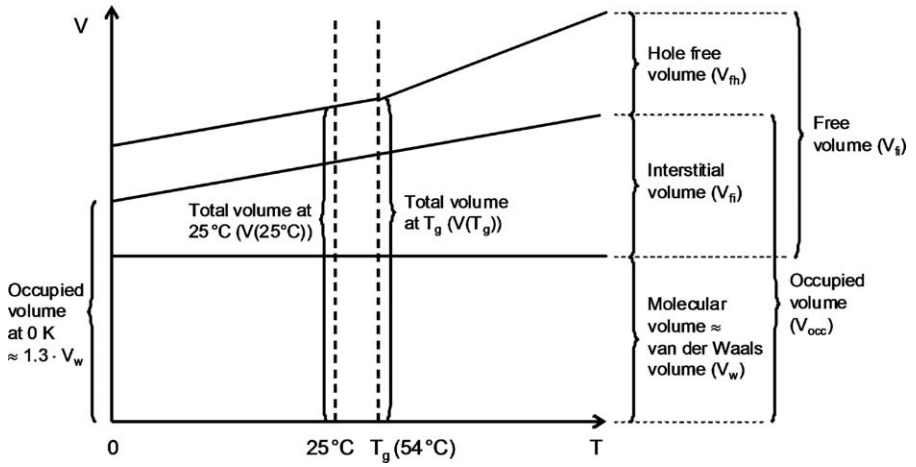

Figure 7. Temperature dependence of the polymer free volume (explanation in the text).

determination of the particle's envelope volume was established to calculate and to compare pore size profiles of different microsphere preparations.[12] In contrast to high-pressure mercury porosimetry, with a lower limit often quoted as about 3 nm, the new method is able to size even subnanometer voids. Table II lists the pore size distribution of the particle preparations B1, B2, B4, B5, and B6, as obtained by the outlined technique. The total pore volume was found to range between 20 and 27% with a volume fraction of about 10–20% being in the micrometer scale. Another fraction of voids is smaller than 2 nm and thus, by definition, represents a micropore space. Particles prepared at 10°C (B1) have a micropore volume of only about 1%. When the extraction temperature is increased to 30°C (B4) and above, the resulting micropore volume rises to about 8–9%. Interestingly, there is a large gap in the pore size range between 0.36 nm and 7.5 μm with only 1% or less of the particle volume distributed in between. Thus, two distinct types of intraparticulate voids can be distinguished: macropores larger than 7.5 μm and subnanopores smaller than 0.36 nm. The existence of voids <0.36 nm could also be proved by small-angle X-ray scattering. These voids in the lower subnanometer range are not pores in the proper sense but can be considered as free volume of the polymer.

Calculation of the Hole Free Volume. The free volume is commonly referred to as the interstitial space between the polymer chains. In contrast to any macroporous voids, it is much more uniformly distributed throughout the polymer matrix, with a maximum size of these intermolecular spaces up to 2 nm, in most cases, however, they are considerably smaller.[19,35] Thus, this cavity system has microporous dimensions by IUPAC definition.[36] The free volume of a polymer can be subdivided into two classes: the interstitial free volume and the hole free volume (= excess free volume) (Figure 7).[35] The interstitial free volume is the major component in a polymer below its glass transition temperature. It is the empty space in a dense packing of molecules (existing also in crystalline materials) and is thus calculated as the difference between the occupied volume and the van der Waals volume (V_w) of the molecules. In amorphous polymers, an additional free volume in the form of small holes appears owing to the static or dynamic structural disorder.[37] Below T_g the hole free volume V_{fh} can be calculated as

$$V_{fh} = V(T_g) f_g \tag{5}$$

with f_g being the fractional free volume at T_g, which is usually 0.025 for the great majority of polymers, and $V(T_g)$ being the total volume of the polymer at T_g, which is the sum of the van der Waals volume of the polymer molecules, the interstitial free volume, and the hole free volume.[38] $V(T_g)$ is obtained from V_w.[39]

$$V(T_g) = (1.3 + 10^{-3} T_g) V_w \tag{6}$$

V_w can be calculated by a group contribution method reported by van Krevelen (and was found to be 0.485 cm^3/g for the polymer employed in this study.[38,40] T_g is the glass transition temperature of dry PLGA (54°C). With the knowledge of V_w and V_{fh}, the interstitial free volume at 25°C (V_{fi}) can be derived as $V_{fi} = V(25°C) - V_w - V_{fh}$. The specific volume at room temperature $V(25°C)$ is obtained as[41]

$$V(25°C) = (1.43 + (0.55 \times 10^{-3} T_g)) V_w \tag{7}$$

For PLGA 75:25, the values of $V(25°C)$, V_{fh}, and V_{fi} were calculated as 0.781, 0.020, and 0.276 cm^3/g, respectively. The occupied volume V_{occ} (= $V_w + V_{fi}$) is 0.761 cm^3/g. Comparing these values with the specific volumes (reciprocal values of the density) of pure PLGA granules, measured by N_2- and He-pycnometry, the value obtained with nitrogen (0.776 cm^3/g) is close to the total volume of the polymer $V(25°C)$ (= $V_{occ} + V_{fh} = 0.781$ cm^3/g), which indicates that nitrogen is hardly able to permeate into the free volume of the polymer. It fills only larger pores, if such exist. In contrast, the helium value (0.768 cm^3/g) lies much closer to V_{occ} (0.761), indicating that helium is able to enter a major part of the hole free volume of the polymer. When looking at preparation B1, with values of 0.782 cm^3/g (N_2) and 0.779 cm^3/g (He), the pycnometric volumes of the microspheres are slightly larger than those of the PLGA raw material, which can be attributed to a larger free-volume space. It is known that the free-volume space of polymers can be expanded by the preparation method of the particles (rate of solvent removal from a polymer solution[19]) or by the steric properties (molecular weight and

degree of branching[35]) of the molecules. However, in case of preparation B1, the He- and the N_2-pycnometric density hardly differs from each other. This indicates the absence of larger dimensioned hole free volume voids, accessible to helium. Interestingly, as the preparation temperature rises from 10 to 35°C (B1→B6) only the pore volume inaccessible to nitrogen increases (B1→B6: N_2: 0.782→0.845 cm^3/g, He: 0.779→0.778 cm^3/g). This indicates an increase of the hole free volume.

Role of the Hole Free Volume in Polymer Hydration. It is known that diffusion can occur if the single cavities of the free volume are equal to or larger than a solvent molecule or a polymer-jumping unit.[38,42,43] Therefore, diffusion processes within a nonmacroporous polymer (or within the scaffold elements of a porous polymer) are mainly controlled by the hole free volume. For a polymer above its T_g, the following equation describes the mathematical relationship between the infinite dilution diffusion coefficient D^{∞} and the hole free volume.[38]

$$D^{\infty} = D_{01} \exp\left(-\frac{\xi V^*}{V_{fh}}\right) \quad (8)$$

V^* is the critical hole free volume for polymer segment motion, which is regarded as the occupied volume at absolute zero. ξ is the coupling parameter and D_{01} is a constant factor related to the energy that a molecule needs to overcome the intermolecular interactions.

Summarizing the findings presented above, the role of the hole free volume in polymer hydration can be explained as follows: If water enters a polymer particle, it first distributes within macropores (where they exist) and within the hole free volume. A first portion of water is imbibed without increasing the mean free volume cavity diameter and consequently without swelling of the polymer matrix.[44] As this water is not free but binds strongly to the polymer, it increases the polymer mobility by disruption of inter- and intra-chain hydrogen bonding and thus decreases the T_g. When the water uptake has reached the point where the T_g falls below the incubation temperature, the polymer changes from the glassy to the rubbery state. The polymer chains gain mobility and allow the water molecules to expand the free-volume cavities, thereby swelling the polymer. As water is a poor solvent of PLGA and the interaction of water molecules with the polymer chains is weaker than the intermolecular forces within the polymer itself, only a limited amount of water participates in the change of the macromolecular structure. Excess water forms a binary system with domains of polymer and free water.[45] Small bulks of free water form inside the cavities which do no longer contribute to plasticization and swelling ceases.[44] Such an interstructural plasticization is characterized by a drop of the T_g to a definite value with no further change upon increase of the plasticizer.[46] This behavior explains the constant value of 36°C in the water-saturated state. Based on this knowledge, it becomes comprehensible that the hole free volume is closely related to the swelling of a polymer. By means of positron annihilation lifetime spectroscopy, Harms et al.[47] could demonstrate with polymer films that a higher free volume is the reason for increased swelling.

DISCUSSION

Evidence for Pore Closure Derived from Drug Release Kinetics

Kinetics of Drug Release. By plotting the logarithm of the initial drug release constant (ln k) versus $1/T$, it can be shown for both preparations, A1 and A2, that between 37 and 60°C the initial rate of drug release increases with the incubation temperature (Figure 2). In this range, the diagram reveals a good proportionality between ln k and $1/T$, indicating that the release mechanism remains unchanged within this temperature range. In contrast, at 32°C the drug release rate is higher than expected which strongly suggests a change of kinetics below 37°C. This temperature limit coincides with the region of the polymer's glass transition temperature, which was found to be 36°C in the fully hydrated state.[26] A similar relationship is also obtained if ln D instead of ln k is plotted against $1/T$ (Figure 3).

The diffusion coefficients are in the range between 10^{-11} and 10^{-14} cm^2/s. This corresponds at least partly to the values reported for the diffusion of other drugs in a PLGA matrix.[48–52] Particularly, the diffusion coefficients of hydrophobic compounds are reported in the literature to have a similar range of temperature-dependent variability. For example, for the hydrophobic dye Bodipy FL in PLGA matrix diffusion coefficients between 4.6×10^{-14} cm^2/s at 22.5°C and 2.7×10^{-11} cm^2/s at 43.0°C were determined.[53]

The temperature dependence of D is able to provide valuable information on the physical state of the diffusion medium. For both study preparations, A1 and A2, above T_g the temperature dependence of the diffusion coefficient is much higher than expected from diffusion in water. In an aqueous solution, the diffusion coefficient D_{liq} should increase by only the factor of 1.6 between 37 and 60°C, as it can be calculated by the Stokes–Einstein equation. This should also be valid as well for the effective diffusion coefficient D_{eff} which describes diffusion through the pore space of porous media, as D_{eff} is proportional to the diffusion coefficient D_{liq} in the liquid medium filling the pores (with the porosity, the constrictivity, and 1/tortuosity being the proportionality factors). However, the experimentally determined diffusion coefficients from preparations A1 and A2 increase by about 1.5 (A1) and 3 (A2) orders of magnitude (30- to 1000-fold) between 37 and 60°C, which gives strong evidence that in the rubbery state the drug diffuses predominantly through the polymer matrix rather than through water filled pores.

In the temperature range above 37°C, the diffusion coefficient D is well described by eq. (1). However, if the incubation temperature drops below T_g, diffusion becomes faster again. As the diffusion in the glassy state of a polymer matrix is generally slower than in its rubbery state, this change in kinetics can be explained only by the appearance of a second more rapid diffusion mechanism, most probably diffusion through water-filled pores. The absence of such pore diffusion above T_g could have its explanation in the absence of a water-filled pore network in the rubbery and thus more swollen state of the polymer.

Kang and Schwendeman[21] studied the release of model drugs (BSA and FITC-dextrin) from PLGA microparticles at incubation temperatures between 4 and 45°C. They also found a faster release at 4 and 25°C than at 37 and 45°C and proposed a significant pore closing at temperatures ≥37°C. Fredenberg et al.[24] confirmed the occurrence of pore closure above T_g by scanning electron microscopical observation of PLGA films incubated at different temperatures. Initially, present pores had disappeared after 2 days at 37 and 45°C, whereas they remained unchanged at 9°C. The underlying mechanism was described to be caused by swelling of the polymer, thus enabling rearrangement of polymer chains and the formation of a homogeneous swollen matrix.[24]

With this strong indication for a disappearance of macropore channels upon hydration of the polymer, the question arises whether this process impedes only the initial drug release from the particles or even the water uptake into the microspheres.

Kinetics of Water Uptake. Figure 4 shows that with rising temperature, despite of an increasing uptake rate, the initial water uptake becomes lower because it ceases earlier. To understand the relationship with the particle structure, the water uptake profiles of preparations B1 and B5 were compared. As mentioned above, these two particle preparations differ from each other in their porosity profile, with only B5 having a significant fraction of micropores. At two time points, 3 and 5 days, the fraction of freezable, unbound water was determined by DSC measurement of the heat of fusion. Comparison with the gravimetrically determined total amount of water revealed that in case of the scarcely microporous preparation B1 even after 5 days the imbibed water is completely unbound. In contrast, the major part of the water taken up by the microporous particles B5 becomes rapidly bound and thus unfreezable (81% after 3 days) and only later the ratio shifts increasingly toward the unbound fraction (29% unfreezable water after 5 days). Similar observations, demonstrating that freezable water does not occur before a first portion of water was incorporated as unfreezable water, were also described in the literature for PLGA 50:50.[54] Hence, the different behaviors of preparations B1 and B5 suggest that the micropores have to be considered to be causative for the fast immobilization of imbibed water. Furthermore, it has to be assumed that during the centrifugation step for separation of the interparticulate water, a portion of the unbound intraparticulate water is removed from the pores. This would explain the relatively low values of total and unbound water in case of the large-pored B1 particles. However, in most experiments values of 20% and more are reached during the first phase of water uptake, which suggests that the whole pore space of the particles (20–27%, see above) becomes filled and is even expanded in some cases. The latter may involve the release of entanglements between the polymer chains in the course of progressive hydrolytic degradation.[54] This may also explain the diminishing water-binding capacity and the decreasing fraction of bound water, as mentioned above. It can be assumed that water uptake comes to stagnation until polymer degradation has reached a certain extent by which a sufficient number of entanglements between the chains are disconnected, thus facilitating further expansion of the particles. As can be seen from a comparison with the degradation profiles (Figure 5), this point is reached at a molecular weight (M_w) of about 25 kDa (after about 10 days), which, however, is still far before the erosional phase of drug release begins (after about 20 days, see below). The curves also reveal that degradation starts immediately after incubation, thus confirming that water enters the particles without any significant delay. Both curves exhibit nearly congruent profiles, which excludes the polymer degradation as a reason for different water uptake and drug release kinetics. Summarizing these results, water uptake can be considered as a very fast process, leading to a complete soaking of the particles and filling of all macroporous voids.[45] In case of micropores being present, water can be distributed rapidly within the polymer matrix and immobilized by binding to the polymer molecules.

Factors and Mechanisms Controlling Pore Closure. In the preceding section, evidence was compiled suggesting a pore closure mechanism being involved in the diffusional drug release from the studied microparticles. It has already been discussed that differences in drug release and water uptake are not caused by differences in polymer degradation. Instead, evidence has been found that the porous structure of the particles may be linked to the release and hydration behavior. To systematically study this hypothesis, a series of particle batches with gradually varying pore structures (Table II) and drug release characteristics (Figure 6) was investigated.

As the size distribution of all six particle batches does not vary in a broad range (Table II), the particle size cannot provide any explanation for the observed differences in drug release behavior. Another well-known factor of influence for drug release is the molecular weight of the polymer in which the drug is embedded. Indeed, a temperature-dependent degradation of PLGA can be observed during microparticle preparation. However, it appears only at temperatures above 30°C. From 10 to 30°C, where the release profile is significantly influenced by the preparation temperature, no degradation is observed during the manufacture but in the temperature range >30°C, where temperature-dependent polymer degradation occurs, the drug release profile remains nearly unchanged (Table II). Thus, it can be concluded that in case of the studied particle batches the influence of the preparation temperature on the drug release behavior is not mediated through the molecular weight of the polymer.

As discussed before with respect to formulations A1 and A2, the fluid transport within the microspheres can take place through a macroporous network whose morphology changes upon swelling of the polymer matrix. Thus, the porous structure could be the key for understanding the dissolution behavior of identically composed but differently manufactured microparticles.

Relationship between Pore Size Distribution and Drug Release. If one tries to correlate the different size fractions of the pore volume (Table II) with the drug release parameters of the particles, a continuous relationship can be found only for the volume of voids <0.36 nm (and for the volume of 0.26–0.36 nm voids, which constitutes the main portion of the voids <0.36 nm). Figure 8 shows the correlation to the amount of

Applied Polymer SCIENCE

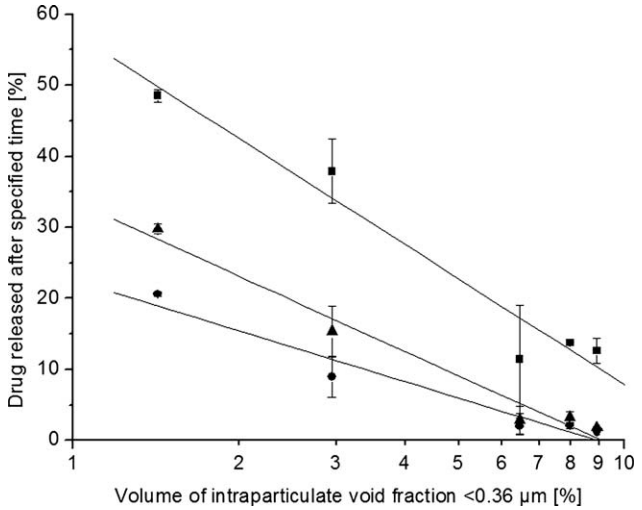

Figure 8. Correlation between drug release after 11 (circles), 14 (triangles), and 21 days (squares) and the volume fraction of intraparticulate voids <0.36 nm.

released drug at three time points (11, 14, and 21 days), all of them in the diffusive phase before polymer erosion begins to dominate the release profile.

For all three release criterions, a linear correlation was found with the logarithm of the void volume fraction <0.36 nm, which was shown to approximately represent the hole free volume. For example, the coefficient of determination R^2 for linear regression of drug release at 14 days on the logarithm of the volume fraction of pores <0.36 nm is 0.97. In contrast, regression of the same drug release parameter on the volume fraction of pores between 0.36 nm and 7.5 µm, on the volume fraction of pores >7.5 µm, and on the volume fraction of the polymer scaffold results in R^2 values of 0.22, 0.27, and 0.17, respectively.

The correlation of the hole free volume with the diffusional part of drug release becomes even clearer when the release curve is decomposed into two additive functions describing the diffusional and the erosional contributions, which was done in a similar way as in the decomposition of the release curves shown in Figure 1. This time, however, to better account for the increasingly pronounced initial lag times in case of higher preparation temperatures, both the diffusional and the erosional release steps were fitted by Weibull terms.

$$m(t) = m_0 + (m_{\max 1} - m_0)\left(1 - \exp\left(-\left(\frac{t - t_{\text{lag1}}}{c_1}\right)^{b_1}\right)\right) + (m_{\max 2} - m_{\max 1})\left(1 - \exp\left(-\left(\frac{t - t_{\text{lag1}} - t_{\text{lag2}}}{c_2}\right)^{b_2}\right)\right) \quad (9)$$

$m(t)$ is the amount of drug released at time t, m_0 is the amount of drug already solved at t_0, $m_{\max 1}$, and $m_{\max 2}$ is the maximum amount of drug released by diffusion and in total, t_{lag1} is the lag time prior to diffusional release and t_{lag2} the lag time between the diffusional and the erosional release phase, c_1 and c_2 are scale constants and b_1 and b_2 are shape constants of the Weibull functions. After calculating the parameters for the best fit of the data, the individual curves of the diffusion and the erosion terms can be plotted as shown in Figure 9.

It is remarkable that, regardless of the particle morphology, the erosional release starts constantly about 20 days after incubation. This can be explained considering the polymer degradation. As shown in Figure 5, independently from the pore structure, the molecular weight reaches a value of about 15 kDa after 20 days. Exactly this value is described in the literature as a critical limit, leading to a spontaneous collapse of the matrix structure, accompanied by an increasing loss of polymer degradation products and embedded drug.[20] Diffusional release starts earlier than erosional release and reaches a maximum value which depends on the preparation conditions and thus on the particle morphology. In case of particles almost completely lacking any hole free volume (B1), it can be seen that diffusion contributes to the release of about 60% of the drug. This is owing to an early onset and a comparably high rate of diffusion, both of which cause a large amount of drug being set free before erosion starts to govern the release. With an increasing fraction of hole free volume, drug release from the particles becomes more and more dominated by polymer erosion. In case of B6, the proportion of drug released by erosion-independent processes has dropped to about 10% because in these particles diffusion starts only shortly before the erosion-driven release phase. Although the latter commences in all preparations after a constant lag time of about 20 days, the onset of diffusional release depends strongly on the pore structure. Thus, the earlier the drug leaks out of the particles by diffusion the larger is the portion which has already left the particles before matrix erosion starts to accelerate the release process.

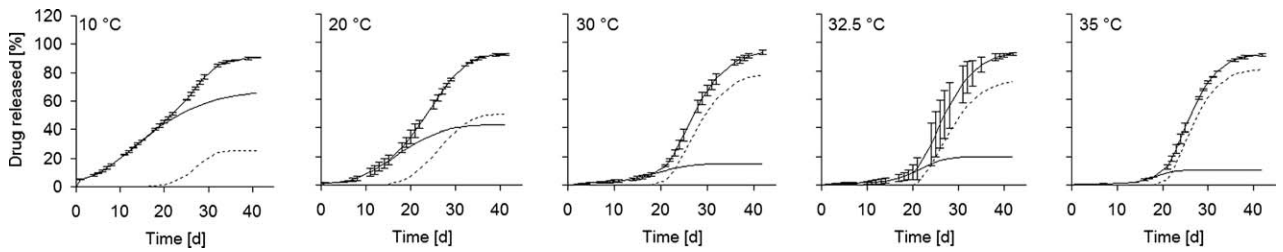

Figure 9. Drug release from preparation B1 to B6 (symbols) fitted by eq. (9) (fitted curves). The solid curves are calculated from the first Weibull term of eq. (9) and depict the contribution of diffusional release. The dotted curves represent the erosional release, computed from the second Weibull term. The measured values (average values and standard deviations) of B1–B3 are based on single batches which were analyzed in duplicate ($n = 2$). The values of B4–B6 are obtained as averages from two batches, produced with identical process parameters, each of them analyzed in duplicate ($n = 4$).

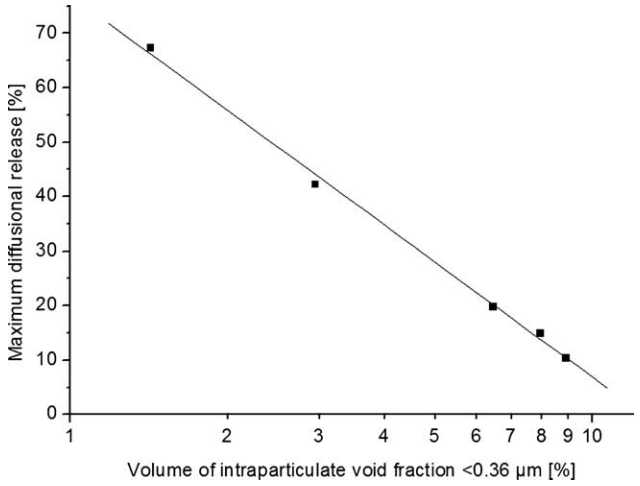

Figure 10. Correlation between the maximum diffusional release and the volume fraction of intraparticulate voids <0.36 nm.

With this knowledge, it is possible to obtain a more accurate measure of the drug fraction released by erosion-independent diffusion. Instead of the more or less erosion-influenced amount released at arbitrarily selected time points within the initial diffusion phase, the calculated m_{max1} values can now be used to describe the total diffusional release unbiased by superimposed erosion effects. Figure 10 shows the highly significant correlation between m_{max1} and the logarithm of the hole free volume (volume of voids, <0.36 nm) ($R^2 = 1.00$).

On the first view, it appears to be a paradox that samples with a higher free volume show a lower diffusional drug release. Faisant et al.,[50] for example, surmised that in lower molecular weight PLGA the diffusion coefficient increases with the free volume available for diffusion. This could also be expected from eq. (8). However, the abovementioned facts are able to provide a possible explanation for the observed inverse relationship.

Proposed Mechanism of Hydration, Swelling, and Drug Release. As shown in Figure 11, it can be assumed that upon incubation water permeates into the dry polymer matrix and spreads rapidly throughout the free volume. Instead of solving the drug and leaching it out, the water becomes immediately immobilized and bound to the polymer. By decreasing the glass transition temperature, it plasticizes the polymer, increases the free volume, and swells the matrix of the microspheres. This volume expansion constricts the interconnected network of macropores which is the main pathway for rapid exchange processes. Hence, inhibiting the release of substances, a closed microclimate inside the spheres is generated. Hydrolysis of the polymer takes place within this microclimate of the sealed particles. As the hydrolysis of PLGA results in the formation of acidic degradation products, the pH within the particles decreases. The early closure of the porous network inhibits the efflux of acids out of the particles. The hydrolysis of the polymer becomes autocatalytically accelerated and erosion of the matrix proceeds from the core to the periphery, hence gradually opening up the particles again and starting the erosive phase of drug release. In this stage also convective and osmotic processes, driven by the polymer degradation products, gain influence and support the increasing diffusion as an additional driving force of drug release.

CONCLUSIONS

Polymer microparticles prepared by emulsification/solvent removal techniques reveal a highly porous structure which can hardly be considered to have the ability to restrict diffusion of water and solved drugs to a significant degree. Nevertheless, in many cases, a more or less pronounced lag time precedes the onset of drug release when the particles are incubated in a test medium. One possible explanation could be the existence of a dense surface layer surrounding the particles which prevents intrusion of water for a certain period of time. However, this hypothesis can be excluded in most formulations, as a certain portion of water is shown to penetrate into the particles already within the first hours after start of incubation and also polymer degradation commences without any delay. Searching for the pathways of water diffusion and drug release, it was found that diffusion through water-filled pores was mainly detectable below the glass transition temperature. Above T_g, when the polymer is in the rubbery state, the measured diffusion coefficients indicate that the drug permeates through the swollen matrix. From vanishing of pore diffusion above T_g, it was concluded that macropores within the particles are constricted when the polymer swells owing to initial water uptake. Drug release profiles were found to be highly dependent on manufacturing conditions but could not be linked to particle size, molecular weight, or overall degree of porosity. Detailed pore size distribution profiles revealed, however, a surprising correlation between the drug release and the volume fraction of voids below 0.36 µm, which

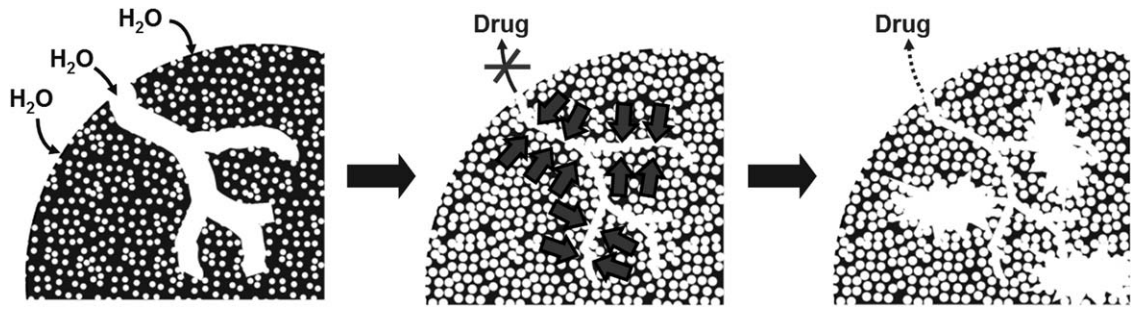

Figure 11. Proposed mechanism of pore closure and delayed drug release by swelling of the hole free volume and resulting constriction of the macropore network.

can be considered to be a measure for the free volume of the polymer. As could be demonstrated by mathematical decomposition of the release profiles, it is solely the diffusional part of drug release which decreases if the hole free volume of the polymer matrix increases. This paradox can be explained with the knowledge that the swelling capacity of polymers is positively correlated to their free volume and that the swollen matrix constricts the network of macroporous voids. By this mechanism, already the first portion water which enters the particles closes the pores and inhibits further water exchange. Hence, the degree of pore closure was shown to depend predominantly on the free volume of the polymer.

ACKNOWLEDGMENTS

The author gratefully acknowledges the assistance received from Mrs. K. Vay in particle preparation and measurement. Thanks are also extended to Mr. M. Noisternig (Institute of Pharmacy, University of Innsbruck) for his support in mercury porosimetry.

REFERENCES

1. Sinha, V. R.; Trehan, A. *J. Control. Release* **2003**, *90*, 261.
2. Zhou, S.; Liao, X.; Li, X.; Deng, X.; Li, H. *J. Control. Release* **2003**, *86*, 195.
3. Eldridge, J. H.; Gilley, R. M.; Staas, J. K.; Moldoveanu, Z.; Meulbroek, J. A.; Tice, T. R. *Curr. Top. Microbiol. Immunol.* **1989**, *146*, 59.
4. Lengsfeld, C. S.; Manning, M. C.; Randolph, T. W. *Curr. Pharm. Biotechnol.* **2002**, *3*, 227.
5. Mathiowitz, E.; Jacob, J. S.; Jong, Y. S.; Carino, G. P.; Chickering, D. E.; Chaturvedi, P.; Santos, C. A.; Vijayaraghavan, K.; Montgomery, S.; Bassett, M.; Morrell, C. *Nature* **1997**, *386*, 410.
6. Sinha, V. R.; Trehan, A. *Crit. Rev. Ther. Drug Carrier Syst.* **2005**, *22*, 535.
7. Gungor, S.; Okyar, A.; Erturk-Toker, S.; Baktir, G.; Ozsoy, Y. *Pharm. Dev. Technol.* **2010**, *15*, 258.
8. El-Baseir, M. M.; Kellaway, I. W. *Int. J. Pharm.* **1998**, *175*, 135.
9. Martínez-Sancho, C.; Herrero-Vanrell, R.; Negro, S. *Int. J. Pharm.* **2006**, *326*, 100.
10. Herrero-Vanrell, R.; Refojo, M. F. *Adv. Drug Deliv. Rev.* **2001**, *52*, 5.
11. von Burkersroda, F.; Schedl, L.; Göpferich, A. *Biomaterials* **2002**, *23*, 4221.
12. Vay, K.; Scheler, S.; Frieß, W. *Int. J. Pharm.* **2010**, *402*, 20.
13. O'Donnell, P. B.; McGinity, J. W. *Adv. Drug Deliv. Rev.* **1997**, *28*, 25.
14. Sansdrap, P.; Moes, A. *J. Int. J. Pharm.* **1993**, *98*, 157.
15. Sturesson, C.; Carlfors, J.; Edsman, K.; Andersson, M. *Int. J. Pharm.* **1993**, *89*, 235.
16. Zolnik, B. S.; Leary, P. E.; Burgess, D. J. *J. Control. Release* **2006**, *112*, 293.
17. Duvvuri, S.; Janoria, K. G.; Mitra, A. K. *J. Control. Release* **2005**, *108*, 282.
18. Cai, C.; Mao, S.; Germershaus, O.; Schaper, A.; Rytting, E.; Chen, D.; Kissel, T. *J. Microencapsul.* **2009**, *26*, 334.
19. Allison, S. D. *Expert Opin. Drug Deliv.* **2008**, *5*, 615.
20. Husmann, M.; Schenderlein, S.; Lück, M.; Lindner, H.; Kleinebudde, P. *Int. J. Pharm.* **2002**, *242*, 277.
21. Kang, J.; Schwendeman, S. *Mol. Pharm.* **2007**, *4*, 104.
22. Wang, J.; Wang, B. M.; Schwendeman, S. P. *J. Control. Release* **2002**, *82*, 289.
23. Fredenberg, S.; Wahlgren, M.; Reslow, M.; Axelsson, A. *Int. J. Pharm.* **2011**, *415*, 34.
24. Fredenberg, S.; Wahlgren, M.; Reslow, M.; Axelsson, A. *J. Control. Release* **2011**, *150*, 142.
25. Mathew, S.; Lendlein, A.; Wischke, C. *Macromol. Symp.* **2011**, 309/310, 123.
26. Vay, K.; Frieß, W.; Scheler, S. *Eur. J. Pharm. Biopharm.* **2012**, *81*, 399.
27. George, S. C.; Thomas, S. *Prog. Polym. Sci.* **2001**, *26*, 985.
28. Arifin, D. Y.; Lee, L. Y.; Wang, C.-H. *Adv. Drug. Deliv. Rev.* **2006**, *58*, 1274.
29. Langenbucher, F. *J. Pharm. Pharmacol.* **1972**, *24*, 979.
30. Kiss, N.; Brenn, G.; Pucher, H.; Wieser, J.; Scheler, S.; Jennewein, H.; Suzzi, D.; Khinast, J. *Chem. Eng. Sci.* **2011**, *66*, 5084.
31. Crank, J. In The Mathematics of Diffusion; Crank, J., Ed.; Clarendon Press: Oxford, **1975**; Chapter *6*, p 89.
32. Siepmann, J.; Siepmann, F. *Int. J. Pharm.* **2008**, *364*, 328.
33. Vay, K.; Scheler, S.; Frieß, W. *Int. J. Pharm.* **2011**, *416*, 202.
34. Koizumi, T.; Panomsuk, S. P. *Int. J. Pharm.* **1995**, *116*, 45.
35. Budd, P. M.; McKeown, N. B.; Fritsch, D. *J. Mater. Chem.* **2005**, 15, 1977.
36. Rouquerol, J.; Avnir, D.; Fairbridge, C. W.; Everett, D. H.; Haynes, J. H.; Pernicone, N.; Ramsay, J. D. F.; Sing, K. S. W.; Unger, K. K. *Pure Appl. Chem.* **1994**, *66*, 1739.
37. Dlubek, G.; Kilburn, D.; Bondarenko, V.; Pionteck, J.; Krause-Rehberg, R.; Alam, M. A. Characterisation of free volume in amorphous materials by PALS in relation to relaxation phenomena. 24. Arbeitskreistagung "Nichtkristalline Strukturen" of DGK, Jena, September 2003. http://www.chemie.uni-jena.0de/DGK-AK4/VOR_03/M_Dlubek.pdf (accessed: February 3, 2013).
38. Lv, H.; Wang, B.; Kong, Y. *Polym. J.* **2009**, *41*, 1049.
39. van Krevelen, D. W. Properties of Polymers; Elsevier: Amsterdam, **1990**; Chapter *4*, p 97.
40. van Krevelen, D. W. Properties of Polymers; Elsevier: Amsterdam, **1990**; Chapter *4*, p 73.
41. van Krevelen, D. W. Properties of Polymers; Elsevier: Amsterdam, **1990**; Chapter *4*, p 95.
42. Cohen, M. H.; Turnbull, D. *J. Chem. Phys.* **1959**, *31*, 1164.
43. Vrentas, J. S.; Duda, J. L. *J. Polym. Sci.: Part B Polym. Phys.* **1977**, *15*, 403.
44. Hodge, R. M.; Bastow, T. J.; Edward, G. H.; Simon, G. P.; Hill, A. J. *Macromolecules* **1996**, *29*, 8137.
45. Blasi, P.; D'Souza, S. S.; Selmin, F.; DeLuca, P. P. *J. Control. Release* **2005**, *108*, 1.

46. Chiang, M. Y. M.; Fernandez-Garcia, M. *J. Appl. Polym. Sci.* **2003**, *87*, 1436.

47. Harms, S.; Rätzke, K.; Faupel, F.; Egger, W.; Ravello, L.; Laschewsky, A.; Wang, W.; Müller-Buschbaum, P. *Macromol. Rapid Commun.* **2010**, *31*, 1364.

48. Wang, F.; Saidel, G. M.; Gao, J. A. *J. Control. Release* **2007**, *119*, 111.

49. Hombreiro-Perez, M.; Siepmann, J.; Zinutti, C.; Lamprecht, A.; Ubrich, N.; Hoffman, M.; Bodmeier, R.; Maincent, P. *J. Control. Release* **2003**, *88*, 413.

50. Faisant, N.; Siepmann, J.; Richard, J.; Benoit, J. P. *Eur. J. Pharm. Biopharm.* **2003**, *56*, 271.

51. Siepmann, J.; Faisant, N.; Akiki, J.; Richard, J.; Benoit, J. P. *J. Control. Release* **2004**, *96*, 123.

52. Kurnik, R. T.; Potts, R. O. *J. Control. Release* **1997**, *45*, 257.

53. Kang, J.; Schwendeman, S. *Macromolecules* **2003**, *36*, 1324.

54. Schmitt, E. A.; Flanagan, D. R.; Linhardt, J. *Macromolecules* **1994**, *27*, 743.